Zurich Open Repository and Archive
University of Zurich
Main Library
Strickhofstrasse 39
CH-8057 Zurich
www.zora.uzh.ch

Year: 2012

Are molecular outflows around high-mass stars driven by ionization feedback?

Peters, Thomas; Klaassen, Pamela D; Mac Low, Mordecai-Mark; Klessen, Ralf S; Banerjee, Robi

Abstract: The formation of massive stars exceeding 10 M sun usually results in large-scale molecular outflows. Numerical simulations, including ionization, of the formation of such stars show evidence for ionization-driven molecular outflows. Here we examine whether the outflows seen in these models reproduce the observations. We compute synthetic ALMA and CARMA maps of CO emission lines of the outflows, and compare their signatures to existing single-dish and interferometric data. We find that the ionization-driven models can only reproduce weak outflows around high-mass star-forming regions. We argue that expanding H II regions probably do not represent the dominant mechanism for driving observed outflows. We suggest instead that observed outflows are driven by the collective action of the outflows from the many lower-mass stars that inevitably form around young massive stars in a cluster.

DOI: https://doi.org/10.1088/0004-637X/760/1/91

Posted at the Zurich Open Repository and Archive, University of Zurich
ZORA URL: https://doi.org/10.5167/uzh-71166
Journal Article

Originally published at:
Peters, Thomas; Klaassen, Pamela D; Mac Low, Mordecai-Mark; Klessen, Ralf S; Banerjee, Robi (2012). Are molecular outflows around high-mass stars driven by ionization feedback? Astrophysical Journal, 760(1):91.
DOI: https://doi.org/10.1088/0004-637X/760/1/91

Draft version September 27, 2012
Preprint typeset using LaTeX style emulateapj v. 5/2/11

arXiv:1209.5858v1 [astro-ph.SR] 26 Sep 2012

ARE MOLECULAR OUTFLOWS AROUND HIGH-MASS STARS DRIVEN BY IONIZATION FEEDBACK?

Thomas Peters[1,2,3], Pamela D. Klaassen[4,5], Mordecai-Mark Mac Low[6], Ralf S. Klessen[1], and Robi Banerjee[7]

Draft version September 27, 2012

ABSTRACT

The formation of massive stars exceeding 10 $M_\odot$ usually results in large-scale molecular outflows. Numerical simulations, including ionization, of the formation of such stars show evidence for ionization-driven molecular outflows. We here examine whether the outflows seen in these models reproduce the observations. We compute synthetic ALMA and CARMA maps of CO emission lines of the outflows, and compare their signatures to existing single-dish and interferometric data. We find that the ionization-driven models can only reproduce weak outflows around high-mass star-forming regions. We argue that expanding H II regions probably do not represent the dominant mechanism for driving observed outflows. We suggest instead that observed outflows are driven by the collective action of the outflows from the many lower-mass stars that inevitably form around young massive stars in a cluster.

1. INTRODUCTION

Jets and outflows always accompany the star formation process, both in the low-mass and in the high-mass regime (Cabrit & André 1991; Bachiller 1996; Reipurth & Bally 2001; Shepherd 2005; Beuther & Shepherd 2005; Arce et al. 2007; Bally et al. 2007; Bally 2007, 2008). Though outflows from low-mass stars are in general understood as resulting from magnetically-driven disk winds during the accretion process, the formation of high-mass outflows from ionizing stars with masses in excess of $10\,M_\odot$ is less understood, as we argue in the next Section, both from the observational (Section 2.1) as well as the theoretical (Section 2.2) point of view.

The recent finding by Peters et al. (2010a) that ionization feedback from massive protostars can drive bipolar molecular outflows has suggested that these could explain the observations of high-mass outflows. In the present paper, we compare the morphology of these molecular outflows with synthetic CO $J = 2-1$ observations (Section 3). We demonstrate that the synthetic observations fail to consistently reproduce observations of molecular outflows in Section 4. In Section 5, we discuss the implications and limitations of this result, and speculate on the actual origin of the observed outflows.

2. OBSERVATIONS AND THEORY OF HIGH-MASS OUTFLOWS

2.1. *Observations of High-Mass Outflows*

Bipolar outflows from high-mass stars are, in many ways, scaled-up versions of their lower-mass counterparts. They do, however, carry significantly more momentum (e.g. Beuther et al. 2002; Wu et al. 2004), and are often less collimated (e.g. Beuther & Shepherd 2005).

Outflows are launched from accretion disks around young stellar objects (e.g. Ray et al. 2007). Disk-like structures have recently also been found around high-mass protostars (Chini et al. 2004, 2006; Beltrán et al. 2004, 2006; Jiang et al. 2008; Davies et al. 2010; Zapata et al. 2010; Motogi et al. 2011), and even in situations where disks cannot be resolved, rotation of the molecular (Howard et al. 1997; Zhang et al. 1998; Klaassen et al. 2009; Galván-Madrid et al. 2009; Beltrán et al. 2011; Furuya et al. 2008, 2011) and ionized (Garay et al. 1986; Sewiło et al. 2008; Keto & Klaassen 2008) gas can still be detected. In many of these regions, bipolar molecular outflows originating from the center of rotation and oriented perpendicular to the rotation have been detected as well, suggesting a causal connection between rotation and outflow.

If high-mass outflows were driven magnetically like their lower-mass analogs, then one would expect a corresponding magnetic field structure along the outflow. Indeed, recent observations suggest a correlation between magnetic field orientation and the presence of outflows from high-mass sources (Girart et al. 2009; Tang et al. 2009a,b, 2010; Vlemmings et al. 2010; Beuther et al. 2010; Surcis et al. 2011). However, whether these maser and dust polarization measurements indicate that the outflows organize the magnetic field or the magnetic field collimates the outflows is less clear.

The momentum and energy imparted to molecular outflows by high-mass protostars scales with the luminosity of the powering source (Richer et al. 2000; Beuther et al. 2002; Arce et al. 2007; López-Sepulcre et al. 2009). Once the high-mass protostar becomes luminous enough to ionize its surroundings, the interaction between outflow and H II region further complicates the picture. Observations suggest that the outflows originate within the ionized gas (De Pree et al. 1994; Galván-Madrid et al. 2009, Klaassen et al. in prep.), and that they can continue into a molecular outflow beyond the ionization bound-

---

tpeters@physik.uzh.ch
[1] Universität Heidelberg, Zentrum für Astronomie, Institut für Theoretische Astrophysik, Albert-Ueberle-Str. 2, D-69120 Heidelberg, Germany
[2] Fellow of the Baden-Württemberg Stiftung
[3] Institut für Theoretische Physik, Universität Zürich, Winterthurerstrasse 190, CH-8057 Zürich, Switzerland
[4] European Southern Observatory, Karl-Schwarzschild-Strasse 2, Garching, Germany
[5] Leiden Observatory, Leiden University, PO Box 9513, 2300 RA Leiden, The Netherlands
[6] Department of Astrophysics, American Museum of Natural History, 79th Street at Central Park West, New York, New York 10024-5192, USA
[7] Hamburger Sternwarte, Gojenbergsweg 112, D-21029 Hamburg, Germany

ary (e.g. K3-50A; De Pree et al. 1994 and Howard et al. 1997).

In order to make statistical arguments about the nature of outflows from protostars of at least intermediate mass, we rely on single dish surveys to characterize their properties. Shepherd & Churchwell (1996) looked at ten sources with bolometric luminosities exceeding 10^2 $L_\odot$ and only found 5 bipolar outflows at a resolution of $60''$, noting that for the other sources, two had multiple velocity components, and the other three had signal to noise ratios too low to draw conclusions from. López-Sepulcre et al. (2009), at a spatial resolution of $11''$, looked at higher luminosity sources ($L_{\rm BOL} > 2\times10^4\ L_\odot$) and found outflows for each of the nine sources they mapped, and strong line wings in the other two sources. Most of these last sources are associated with H II regions. Qin et al. (2008) studied the gas motions from 15 high-mass star forming regions with ultracompact H II regions and found evidence for outflows towards 10 of them. However, at a spatial resolution $> 1'$, this detection fraction should be used as a lower limit. The five sources without outflows were amongst the nearest sources in their survey, suggesting that distance did not play a role in the non-detections. In each of these studies, outflow masses range from 3 to 10^3 $M_\odot$, and their energies are of the order 10^{46} erg or greater.

With interferometers one gains a better understanding of which source is responsible for the large-scale outflows seen in the single dish surveys. With current instruments we are limited in the number of sources for which detailed analyses can be performed. Nonetheless, in-depth observations have been made by many groups in an attempt to better understand the powering sources and their relationships with their environments. Generally, these high resolution ($\lesssim 1''$) studies show that the outflow originates at the brightest continuum object in the field. These sources include: G29.96 (Beltrán et al. 2011), G24.78A (Furuya et al. 2002), W51e2 (Keto & Klaassen 2008; Shi et al. 2010), G5.89 (Acord et al. 1997; Watson et al. 2007; Hunter et al. 2008), NGC 7538 IRS 1 and G28.2 (Klaassen et al. 2011), G31.41 (Olmi et al. 1996a,b), G75.78 and G75.77 (Riffel & Lüdke 2010).

In many of these sources, rotation of the warm gas surrounding the H II region has also been detected perpendicular to the outflow direction (see Beltrán et al. 2006, 2011; Klaassen et al. 2009; Olmi et al. 1996b,a, etc.).

Keto & Klaassen (2008) and Klaassen et al. (2011) showed that molecular outflows appear at the edges of the H II regions already at high velocities, suggesting these outflows are powered from within the H II region. In fact, the radio recombination line study of De Pree et al. (1994) displayed velocity shifts in this ionized gas tracer from K3-50A, suggesting an ionized outflow. The molecular observations of Howard et al. (1997) are consistent with this outflow penetrating the ionization boundary and continuing as a molecular outflow. Observations of ionized outflow lobes have also been reported for G48.75 (Johnston et al. 2009). Furthermore, Cesaroni et al. (2010) discuss the possibility that the outflow in G31.41 originates from an ionized jet, and Guzmán et al. (2011) suggest that an ionized jet in IRAS 16562-3959 is the energy source of a molecular outflow in the same region.

2.2. *Possible Outflow Driving Mechanisms*

We now consider the problems with existing explanations of outflow driving. Protostellar outflows around low-mass protostars are generally attributed to magnetic fields, either through the launching of disk winds (Blandford & Payne 1982; Pudritz & Norman 1983; Ouyed & Pudritz 1997; Krasnopolsky et al. 1999; Königl & Pudritz 2000; Fendt & Čemeljić 2002; Fendt 2006), magnetic tower flows (Tomisaka 1998, 2002; Lynden-Bell 2003; Matsumoto & Tomisaka 2004; Machida et al. 2004; Banerjee & Pudritz 2006, 2007; Seifried et al. 2012) or through the interaction between the protostellar magnetosphere and the disk field (Najita & Shu 1994; Shu et al. 1994, 2007; Cai et al. 2008; Lovelace et al. 1999; Romanova et al. 2009). Recently, the applicability of these driving mechanisms in the high-mass regime has been questioned (Peters et al. 2011) on the grounds that severe gravitational instability in the accretion flow surrounding the massive star destroys the coherent rotational motion in the disk plane that is required for all these models to work, and the ionization feedback disrupts the magnetic field structure. The statistical distribution of orbital separations with a peak at a semimajor axis of ~ 0.15 AU found by Kobulnicky & Fryer (2007) in the massive binary data of Garmany et al. (1980) suggests that the inner disk region is gravitationally unstable as well, making magnetic jet launching very difficult. Furthermore, magnetically driven jets around low-mass stars may be collimated at the disk-magnetosphere boundary (Lii et al. 2012), and massive stars are known to have relatively weak magnetospheres compared to low-mass stars (e.g. Owocki 2009). To fully model this process we need to resolve the inner disk region (radii less than 1 AU) where magnetic launching is expected. This will require high-resolution radiation-magnetohydrodynamical calculations that connect the larger-scale gravitationally unstable accretion flow (radii of several thousand AU) to the inner disk region.

Vaidya et al. (2009, 2011) tried to fill this gap in two-dimensional calculations that include both ideal magnetohydrodynamics as well as the effects of radiative pressure in the line-driving approximation. They find that initially well collimated outflows can widen up as the central star grows in mass and its luminosity increases. This could explain the observational proposal that more evolved outflows around massive stars have larger opening angles than very young ones (Beuther & Shepherd 2005). Because of the restricted geometry in the Vaidya et al. work, however, these studies cannot consider the effects of disk fragmentation, so further analysis is required. A more consistent treatment of the complex interplay between the fragmentation behavior of the inner disk, magnetic fields, and radiative processes has been presented by Commerçon et al. (2011). Their three-dimensional radiation-magnetohydrodynamics calculations indicate that magnetic braking efficiently removes angular momentum from the disk, leading to high accretion rates and luminosities. This heats the disk and reduces the degree of fragmentation at small radii. Because these calculations are prohibitively expensive, they could not follow the evolution into the realm of massive stars where ionizing radiation becomes important. This regime has been covered by Peters et al. (2011)

with somewhat lower resolution. They find that magnetic fields cannot completely suppress fragmentation at large disk radii (see also Hennebelle et al. 2011).

Additional evidence against magnetic driving mechanisms comes from the notable lack of observations of extremely high-velocity jets associated with high-mass outflows. Since magnetically launched jets form deep within the gravitational potential well around the star, and the potential well around high-mass stars is deeper than around low-mass stars, jets would be expected with velocities comparable to those of line-driven stellar winds, exceeding $1000\,\mathrm{km\,s^{-1}}$. Instead, the observed structures never propagate faster than jets from low-mass stars. However, even if there were very high-velocity jets, they might be immediately slowed by interaction with the accretion flow, which is expected to be stronger for high-mass than for low-mass stars.

Radiation pressure on the accretion flow could also drive outflows. Krumholz et al. (2009) used a gray flux-limited diffusion method to simulate this effect. They found that the radiation pressure creates bubbles around the massive star that get destroyed by Rayleigh-Tayor instabilities. These radiation bubbles are morphologically dissimilar to molecular outflows. Additionally, by the time the bubbles form, the star would be massive enough to ionize the interior of the bubble, so that the bubble would become an H II region and not be molecular anymore. Kuiper et al. (2011), using a frequency-dependent treatment of the direct stellar radiation combined with gray flux-limited diffusion, do not see these Rayleigh-Tayor instabilities. As possible reasons for this difference they suggest a better modeling of the first absorption of photons with their numerical scheme, but it could also be that they will see the instability once their bubbles reach the same size as those of Krumholz et al. (2009) or that their density distribution has led to a decelerating, thus stable, bubble. A more recent study (Kuiper et al. 2012), in which both the frequency-dependent treatment and gray flux-limited diffusion are applied to the same initial conditions, seems to confirm that the instability is an artifact caused by the gray approximation of the direct stellar radiation. In any case, ionization would also fill the stable radiation-driven bubbles of Kuiper et al. (2011, 2012) with ionized gas, so that stable radiation pressure-driven outflows cannot account for the observed high-mass molecular outflows either.

Another source of momentum is line-driven winds of high-mass stars (e.g. Castor et al. 1975). Indeed, some of the observations show high-mass outflows that are poorly collimated and seem to be consistent with being wind-blown bubbles (e.g. Shepherd 2005; Beuther & Shepherd 2005). However, typical massive outflows have momentum fluxes that are two orders of magnitude higher than those produced by stellar winds (e.g. Richer et al. 2000). Hence, stellar winds cannot be the primary drivers of high-mass outflows already for reasons of momentum conservation, and they are certainly not responsible for the more collimated outflows found in earlier phases of high-mass star formation (e.g. Beuther et al. 2002).

Recently, Peters et al. (2010a) have shown that ionization feedback can drive bipolar molecular outflows. Contrary to classical understanding of H II region growth, these simulations show that the H II regions around massive protostars do not expand monotonically as long as the high-mass star is still embedded in an accretion flow. Instead, the H II region flickers whenever the ionizing radiation gets shielded by dense filaments formed in the gravitationally unstable accretion flow (Galván-Madrid et al. 2011). This rapid fluctuation of the thermal gas pressure drives bipolar molecular outflows parallel to the net angular momentum vector: the pressure increase during the ionization process drives the material away from the density enhancement in the plane of rotation, and the subsequent recombination lets the blown-out material become a molecular outflow.

3. SYNTHETIC ALMA OBSERVATIONS

We use synthetic ALMA observations of CO to characterize the ionization-driven outflows found by Peters et al. (2010a). We describe the input models (Section 3.1) and the CO emission maps (Section 3.2).

3.1. *Input Models*

The simulations use an extended version of the adaptive-mesh numerical hydrodynamics code FLASH (Fryxell et al. 2000) with sink particles (Federrath et al. 2010) to follow the collapse beyond the formation of the first objects, allowing us to describe the early evolution of the disk that builds up, and our improved hybrid characteristics raytracing method (Rijkhorst et al. 2006; Peters et al. 2010a) that propagates the ionizing and non-ionizing radiation on the grid. We refer to Peters et al. (2010a) for details on the numerical algorithm and initial conditions. A thorough description of the spatial and temporal H II region evolution in these simulations can be found in Peters et al. (2010a), Peters et al. (2010c) and Galván-Madrid et al. (2011).

We analyze two simulations. Both simulations start from a $1000\,M_\odot$, spherical molecular cloud of diameter 3.2 pc. The cloud is initially in solid body rotation with angular velocity $\omega = 1.5 \times 10^{-14}\,\mathrm{s^{-1}}$. During the collapse of this massive core, a rotationally flattened structure forms that quickly becomes gravitationally unstable and fragments. In one simulation (Run B), we form a full stellar cluster in this rotating accretion flow, including radiative feedback by both ionizing and non-ionizing radiation. In another simulation (Run A), also including radiation feedback, we artificially prevent the formation of all stars after the first one and run the simulation with a single star only. In Run B, three massive stars with masses around $20\,M_\odot$ form, each creating an H II region around itself, along with numerous lower mass stars. In contrast, the star in Run A reaches more than $70\,M_\odot$. A thorough discussion of the effects of radiative feedback and the suppression of fragmentation can be found in Peters et al. (2010a,b).

The massive stars in both simulations drive bipolar outflows with their ionization feedback. The basic mechanism, as already mentioned in Section 2.2, is the repeated shielding of the ionizing radiation by dense streams of gas in the accretion flow around the massive star. The ionizing radiation accelerates the molecular gas around the H II region down the steepest density gradient, perpendicular to the rotational flattening. When the ionizing radiation gets shielded by the filamentary accretion flow, the ionized gas can recombine on timescales as short as $\sim 100\,\mathrm{yr}$, and then the outflow becomes molecular, given that the formation timescale of molecular hydrogen in these dense outflows is less than a year (Hollenbach et al. 1971). The molecular outflow continues to expand by momentum conservation. Since the outflow is not driven anymore without the thermal pressure of the ionized gas, the outflow can escape from the gravitational potential well of the stellar cluster only if its initial velocity permits. After the loss of thermal support, the outflow decelerates and eventually falls back onto the rotationally flattened structure by its gravitational attraction. The online material of Peters et al. (2010a) contains movies of density slices showing this process for both runs.

Generally, the outflows in Run A are much more powerful than the outflows in Run B. The reasons are the stronger accretion flow in which the massive star is embedded and the larger ionizing luminosity. Though Run A is not a realistic model of massive star formation globally, the driving of the molecular outflow by the interaction of the ionizing radiation with the accretion flow is modeled correctly. These stronger accretion flows could be realized in simulations with multiple stars by, for example, starting from a more massive core, using a more centrally concentrated density profile (e.g. Girichidis et al. 2012), or reducing the initial rotational motion of the core (e.g. Seifried et al. 2011).

The online material for this article contains animations of the ionization-driven outflows for both simulations. The videos show volume renderings of gas density (left) and thermal pressure (right). The direct comparison of the two images allows the identification of the H II regions and illustrates how the thermal pressure of the ionized gas drives the molecular fountains. For comparison, we also show an animation of a third simulation, Run E (see Peters et al. 2011), in which an additional large-scale outflow is driven by magnetic fields and interferes with the ionization-driven outflows. Though the interplay between the different types of outflows is highly complex, the morphological differences between the magnetically-driven outflows and the ionization-driven outflows becomes very clear.

3.2. *CO Emission Maps*

We have previously used the three-dimensional adaptive-mesh radiative transfer code RADMC-3D[8] to generate maps of free-free and dust emission from our simulation data (Peters et al. 2010c). Here we use the capability of RADMC-3D to model molecular line emission (e.g. Shetty et al. 2011). In order to trace the bulk dynamics of the gas, we have chosen to model the CO $J = 2-1$ transition at 230.538 GHz. We have simulated observing the outflows at a distance of 1.3 kpc, the same distance as G5.89-0.39 (Motogi et al. 2011). This source is believed to be powered by a 25 $M_\odot$ star, and is so directly comparable with one of the stars in Run B.

CO is an excellent tracer of the bulk gas dynamcis in star-forming regions because of its relatively low critical density, and relatively high abundance (10^{-4} with respect to molecular hydrogen, Wilson & Rood 1994). It is the most abundant molecule after H_2 and is therefore a good tracer of large-scale structures. Its low critical density means that it is detected even in the tenuous high-velocity gas in outflows. SiO, another excellent outflow tracer, was not used because it emits on much smaller scales and its emission is directly tied to the type of shocks produced in the outflow (i.e. Si is liberated from dust grains by sputtering during the extended passage through C-shocks mediated by ion-neutral drag, but not by classical J-shocks (Schilke et al. 1997; Gusdorf et al. 2008; Guillet et al. 2011)).

For simplicity, we assume local thermodynamic equilibrium (LTE) conditions. We use the CO Einstein coefficients from the Leiden Atomic and Molecular Database (Schöier et al. 2005). These 3D data cubes were then converted into skymaps, and observations with ALMA were simulated using the "simobserve" and "simanalyze" tasks in CASA 3.4 (McMullin et al. 2007). The native resolution of the original datacube was 49 AU. Assuming the source was at the distance of 1.3 kpc, this gives a native resolution of 0.038". This is much higher than the final resolution achieved in our ALMA simulations. We simulated observing with ALMA in a moderately high resolution mode ("alma.out10.cfg"), achieving a resolution of 0.5" at 230 GHz with a channel spacing of 1 km s^{-1}. The rms sensitivity for the ALMA observations should be 1.2 mJy/beam for a 0.5" beam. Noise was added in the UV plane to simulate $4^{\rm th}$ quartile observing conditions. We also simulated observing with CARMA in its C configuration. This resulted in a final image resolution of 1.3" $\times$ 1.0". The CASA simulator assumed a system temperature of 200 K for the CARMA observations. For all simulations, we assumed a total integration time of four hours. For the ALMA mosaic, we required six pointings, and with CARMA, two.

Cleaning was done non-interactively using natural weighting and a 3 σ cutoff. Zeroth and first moment maps were created using line wing emission, excluding emission from within 3 km s^{-1} of the source rest velocity. The zeroth moment (integrated intensity) maps were used to compute the column density following the procedure described in Klaassen et al. (2011), assuming a temperature of $T = 100\,$K. Because the size of the emitting region can be determined from the images, the number of molecules was calculated from the column density assuming a CO abundance of 10^{-4} with respect to H_2. From this, the gas mass was determined (see the first column of Table 1). From the first moment (intensity weighted velocity) maps, characteristic velocities of the outflowing gas were derived. These values are presented in the second column of Table 1. The uncertainties in Table 1 reflect the noise output from the ALMA observation simulator which were propagated (in quadrature) through the equations used to derive the outflow properties.

Outflow momentum was calculated from $P = mv$, and energy from $E = 0.5mv^2$. Outflow luminosities and mass loss rates were determined by dividing the outflow energies and masses by the kinematic age of the outflows (400 yr). More details on this type of calculation can be found in Klaassen et al. (2011). For each of our modelled outflows, we find that many outflow properties as measured by ALMA are about a factor of two higher than those observed with CARMA.

Figures 1 and 2 show three color images of the CO emission for snapshots of Run A and Run B as would be

---

[8] http://www.ita.uni-heidelberg.de/~dullemond/software/radmc-3d/

TABLE 1
Outflow parameters derived from CARMA and ALMA simulations

CARMA		M ($M_\odot$)	V (km s^{-1})	P ($M_\odot$ km s^{-1})	E (10^{44} erg)	L ($L_\odot$)	$\dot{M}$ (10^{-3} $M_\odot$ yr^{-1})	R (AU)
Run A	blue	0.059±0.001	3.816±0.126	0.224±0.010	0.085±0.007	0.175±0.048	0.147±0.031	4100
	red	0.066±0.001	3.391±0.150	0.223±0.012	0.075±0.007	0.155±0.046	0.165±0.035	4100
Run B (left)	blue	0.013±0.000	3.634±0.199	0.048±0.004	0.017±0.002	0.036±0.012	0.033±0.007	3300
	red	0.060±0.000	3.318±0.199	0.198±0.013	0.065±0.008	0.134±0.044	0.149±0.031	2100
Run B (right)	blue	0.058±0.000	3.549±0.140	0.206±0.009	0.073±0.006	0.150±0.043	0.145±0.030	5000
	red	0.034±0.000	2.453±0.000	0.082±0.001	0.020±0.000	0.041±0.009	0.084±0.018	4100
ALMA		M ($M_\odot$)	V (km s^{-1})	P ($M_\odot$ km s^{-1})	E (10^{44} erg)	L ($L_\odot$)	$\dot{M}$ (10^{-3} $M_\odot$ yr^{-1})	R (AU)
Run A	blue	0.082±0.000	3.888±0.099	0.320±0.009	0.124±0.007	0.255±0.065	0.206±0.042	4100
	red	0.101±0.000	3.297±0.154	0.333±0.016	0.109±0.010	0.225±0.066	0.252±0.051	4100
Run B (left)	blue	0.050±0.000	3.446±0.000	0.171±0.001	0.059±0.000	0.121±0.025	0.124±0.025	3300
	red	0.141±0.000	2.757±0.184	0.388±0.026	0.106±0.014	0.219±0.073	0.352±0.071	2100
Run B (right)	blue	0.060±0.000	3.550±0.143	0.213±0.009	0.075±0.006	0.155±0.044	0.150±0.030	5000
	red	0.044±0.000	2.370±0.000	0.104±0.000	0.024±0.000	0.050±0.010	0.109±0.022	4100

Note. — The table shows the mass M, velocity V, momentum P, kinetic energy E, mechanical luminosity L, mass-loss rate $\dot{M}$, and size R of the observed outflows for two snapshots in Run A and Run B. The kinematic age of all outflows is 400 yr.

observed with CARMA and ALMA, respectively, after being processed through CASA. The images were observed at an inclination of 30° with respect to the disk normal direction, which is a typical orientation (Cabrit & Bertout 1986). The zeroth moment maps of the blue and red shifted emission were cut at 3 σ for this plot (as shown in blue and red, respectively). The white areas correspond to the brightest regions in the map, the position of the high-mass protostar. The two outflows visible in the map for Run B are driven by two separated massive stars, one of which still has a small H II region (right), while the H II region around the other star has totally recombined (left). As the stars move through the flattened structure, their ionizing radiation continuously drives material out perpendicular to it, but after the star has moved and the gas has recombined, the gas falls back. This process creates a large-scale molecular fountain, but its velocity is smaller than our low-velocity cut-off, and the interferometer additionally filters out some of its large-scale structure. Hence, the map only shows the smaller, more powerful outflows that are currently driven by the ionization feedback from the massive stars, and not the large-scale bubble that is also present.

4. DISCUSSION

4.1. *Comparison to exact solution*

We can calculate the mass, momentum and kinetic energy in the outflows exactly. To this end, we use RADMC-3D to sum over the mass, momentum and energy in zones with velocity high enough to be contained in the outflow as viewed along the line of sight of the simulated observation. We only take cells with $3\,\mathrm{km/s} \leq v \leq 7\,\mathrm{km/s}$ into account, which corresponds to the selection criterion used with the synthetic maps. The results of these direct measurements are listed in Table 2. The directly measured values are comparable with the numbers inferred from the synthetic observations, but generally higher. The reason could be that the synthetic observations do not recover all the flux from the outflows.

The morphology of the outflow for Run A as pictured in Figure 2 suggest that the outflow is pointing mostly along the line of sight to the observer, which can be confirmed by examining the raw simulation data. This finding is also supported by the intensity-weighted velocities (characteristic velocities, listed in Table 1) of the gas in this outflow, which are slightly higher than those for the outflows in Run B. The morphology of the two outflows in the figure for Run B (along with their lower characteristic velocities) suggest they are more likely oriented closer to the plane of the sky, which is again confirmed by the raw data. However, the ionizing luminosity that powered these outflows before the H II region recombined is also vastly different: the star in Run A has 57 $M_\odot$, while the two massive stars in Run B have masses around 20 $M_\odot$ each.

Our analysis shows that the flickering of the ionization feedback can produce molecular outflows that are morphologically similar to but smaller than the observed ones. They appear to be very young compared to the age of the star because they are not driven continuously. Because of their short kinematic age, the momentum, energy and luminosity of the outflows are relatively small compared to observed outflows around high-mass stars. We predict that these small, high-momentum, but low-velocity outflows will be found by upcoming ALMA observations that probe the driving sources of high-mass outflows, if they can be disentangled from the larger high-velocity outflows.

4.2. *Comparison to observations*

The outflows in Figure 2 are smaller than those generally seen in high-mass star forming regions. However their kinematic ages ($\sim$ 400 yr) suggest they are also much younger than those which have been observed to date. These two properties are presumably correlated. Although the calculated outflow masses and kinematic properties (momentum, energy and mechanical luminosity) are consistent with the range of these properties found for high-mass star-forming regions (e.g. Wu et al. 2004), they are located near their lower boundaries.

We find the outflow velocities in the simulations to

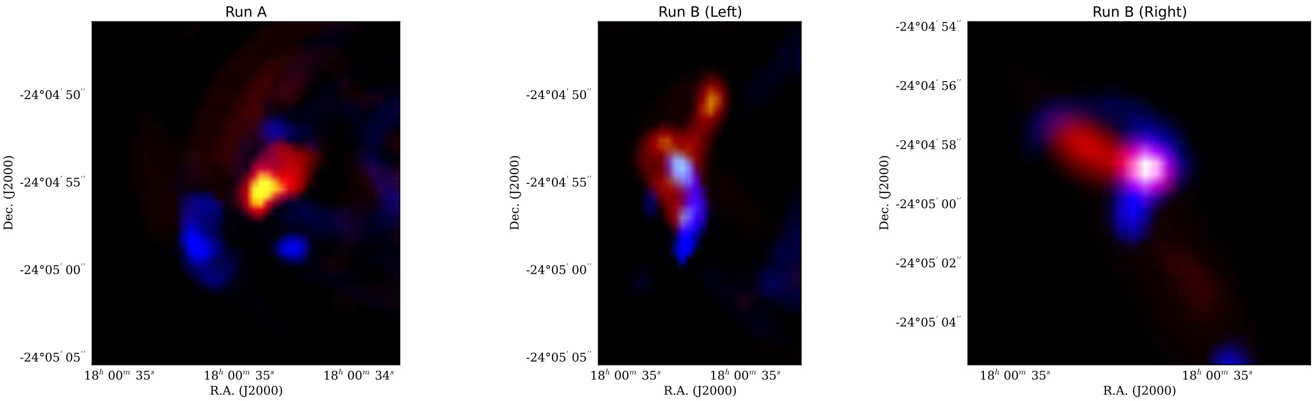

Fig. 1.— Three color images of synthetic CARMA observations of snapshots from Run A and Run B processed with CASA. The resolution of these observations is 1.3” × 1.0”, and the two point mosaic was simulated to have been observed for four hours on source. Noise was added in the UV plane to simulate a system temperature of 200 K, and the source was assumed to be at the distance of G5.89 (1.3 kpc).

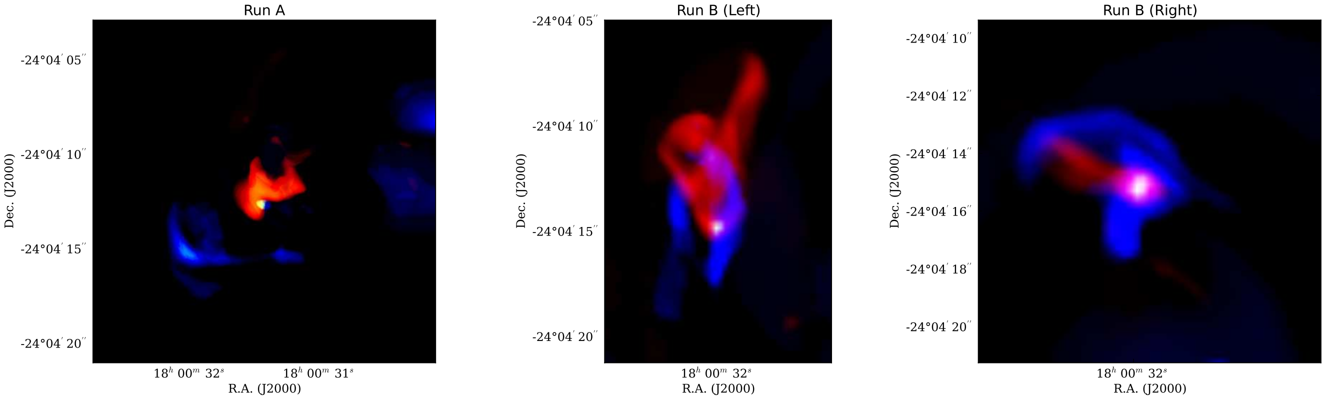

Fig. 2.— Three color images of synthetic ALMA observations of snapshots from Run A and Run B processed with CASA. The resolution of these observations is 0.5″, and the six point mosaic was simulated to have been observed for four hours on source. Noise was added in the UV plane to simulate fourth quartile observing conditions, and the source was assumed to be at the distance of G5.89 (1.3 kpc).

be an order of magnitude smaller than those in G5.89 even though previous observations of this source (e.g. Puga et al. 2006; Su et al. 2012) were at similar angular resolutions.

The simulated mass infall rates are high compared to observations if we assume all of the infalling mass makes it onto the central forming star ($\dot{M}_{\mathrm{in}} \sim 10^{-3}\ M_{\odot}\ \mathrm{yr}^{-1}$ suggests a 10 $M_{\odot}$ star forms in 10^4 yr), however much of the infalling material will not be accreted by the central star(s). Instead, secondary stars form in the gravitationally unstable accretion flow around the massive star and intercept gas that would otherwise fall inwards in a process called fragmentation-induced starvation (Peters et al. 2010a,b; Girichidis et al. 2012).

TABLE 2
Outflow parameters derived from direct measurements

		M ($M_{\odot}$)	P ($M_{\odot}$ km s^{-1})	E (10^{44} erg)
Run A	blue	0.67	2.43	0.91
	red	1.49	5.84	2.44
Run B (left)	blue	0.04	0.18	0.08
	red	0.23	0.90	0.38
Run B (right)	blue	0.13	0.53	0.23
	red	0.04	0.17	0.07

Note. — Outflow mass M, momentum P and kinetic energy E as directly measured from the simulation data.

5. CONCLUSIONS

Our results show that ionization feedback is able to drive molecular outflows around high-mass stars that have properties consistent with some observed ones. However, the measured properties are rather on the lower boundary of the typical values of high-mass outflows, which makes it unlikely that ionization feedback is the main driver of high-mass outflows. Additional feedback mechanisms like radiation pressure and stellar winds or magnetic fields might help, but as discussed in the Introduction, there is no strong evidence that this is indeed the case.

We note, however, that lower-mass companions naturally form with high-mass stars in their gravitationally unstable accretion flow (Peters et al. 2010a,b, 2011; Girichidis et al. 2012), in agreement with the observation that massive stars are typically found as members of higher-order multiple stellar systems and clusters (Ho

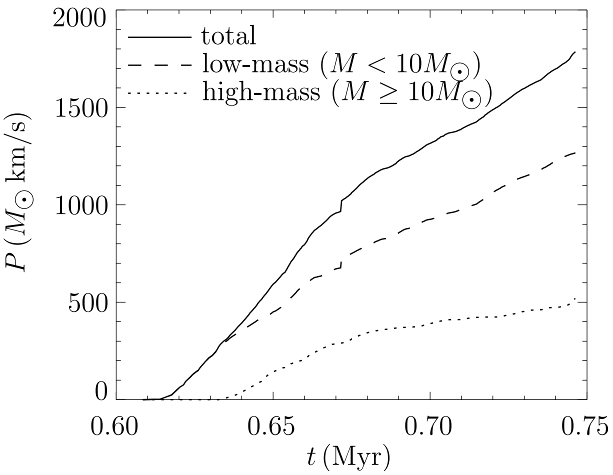

Fig. 3.— Momentum input P according to the outflow model from the stars in the cluster as function of time t. The joint momentum injected by the low- and intermediate-mass stars is well within the regime of high-mass outflows.

& Haschick 1981; Zinnecker & Yorke 2007). We propose that it is the joint outflow activity of the low- and intermediate-mass companions that we are seeing.

We tested whether the low- and intermediate-mass companions in the accretion flow around the massive stars in our simulations at least in principle are able to reproduce the characteristics of high-mass outflows with a simple model. We assume that a factor of $f = 0.1$ of the accreted material onto the stars is ejected again as an outflow with an initial velocity of $v_\mathrm{wind} = 150\,\mathrm{km\,s^{-1}}$ (e.g. Bontemps et al. 1996). The momentum injected into the surrounding gas by a single star per unit time is then $\dot{P} = f\,v_\mathrm{wind}\,M_\mathrm{acc}$ for an accretion rate M_acc. Figure 3 shows the integrated total momentum P as function of time for all stars in the cluster.

The figure shows that even with conservative assumptions the low- and intermediate-mass stars alone can easily produce outflow momenta in the regime of observed high-mass outflows. Their contribution is orders of magnitude larger than the momentum in the ionization-driven outflows.

Further simulations that simultaneously include ionization feedback from massive stars as well as the mechanical feedback from their low- and intermediate-mass companions are required to thoroughly test this proposal.

ACKNOWLEDGEMENTS

We thank Herwig Zilken from the Jülich Supercomputing Centre for his help with visualizing our simulation data. We also thank the anonymous referee for useful comments that helped to improve the paper. T.P. acknowledges financial support as a Fellow of the Baden-Württemberg Stiftung funded through contract research under grant P-LS-SPII/18 in their program *Internationale Spitzenforschung II* and through SNF grant 200020_137896. M.-M.M.L. was partly supported by NSF grant AST 11-09395. R.S.K. acknowledges funding from the *Deutsche Forschungsgemeinschaft* DFG via grants KL 1358/14-1 as part of the Priority Program SPP 1573 *Physics of the Interstellar Medium* as well as via the Collaborative Research Project SBB 811 *The Milky Way System* in subprojects B1, B2, and B4. R.B. acknowledges funding from the DFG via the grant BA 3706/1-1. We acknowledge computing time at the Leibniz-Rechenzentrum in Garching, the Texas Advanced Computing Center through grant TG-MCA99S024 from the Extreme Science and Engineering Discovery Environment (XSEDE), which is supported by the National Science Foundation grant number OCI-1053575, and at Jülich Supercomputing Centre. The FLASH code was in part developed by the DOE-supported Alliances Center for Astrophysical Thermonuclear Flashes (ASCI) at the University of Chicago.

REFERENCES

Acord, J. M., Walmsley, C. M., & Churchwell, E. 1997, ApJ, 475, 693
Arce, H. G., Shepherd, D., Gueth, F., et al. 2007, in Protostars and Planets V, ed. B. Reipurth, D. Jewitt, & K. Keil (Tucson: The University of Arizona Press), 245
Bachiller, R. 1996, ARA&A, 34, 111
Bally, J. 2007, Ap&SS, 311, 15
Bally, J. 2008, in Astronomical Society of the Pacific Conference Series, Vol. 387, Massive Star Formation: Observations Confront Theory, ed. H. Beuther, H. Linz, & T. Henning, 158
Bally, J., Reipurth, B., & Davis, C. J. 2007, in Protostars and Planets V, ed. B. Reipurth, D. Jewitt, & K. Keil (Tucson: The University of Arizona Press), 215
Banerjee, R., & Pudritz, R. E. 2006, ApJ, 641, 949
—. 2007, ApJ, 660, 479
Beltrán, M. T., Cesaroni, R., Codella, C., et al. 2006, Nature, 443, 427
Beltrán, M. T., Cesaroni, R., Neri, R., & Codella, C. 2011, A&A, 525, A151
Beltrán, M. T., Cesaroni, R., Neri, R., et al. 2004, ApJ, 601, L187
Beuther, H., Schilke, P., Sridharan, T. K., et al. 2002, A&A, 383, 892
Beuther, H., & Shepherd, D. 2005, in Cores to Clusters: Star Formation with Next Generation Telescopes, ed. M. S. N. Kumar, M. Tafalla, & P. Caselli (Springer-Verlag), 105
Beuther, H., Vlemmings, W. H. T., Rao, R., & van der Tak, F. F. S. 2010, ApJ, 724, L113
Blandford, R. D., & Payne, D. G. 1982, MNRAS, 199, 883
Bontemps, S., André, P., Terebey, S., & Cabrit, S. 1996, A&A, 311, 858
Cabrit, S., & André, P. 1991, ApJ, 379, L25
Cabrit, S., & Bertout, C. 1986, ApJ, 307, 313
Cai, M. J., Shang, H., Lin, H.-H., & Shu, F. H. 2008, ApJ, 672, 489
Castor, J. I., Abbott, D. C., & Klein, R. I. 1975, ApJ, 195, 157
Cesaroni, R., Hofner, P., Araya, E., & Kurtz, S. 2010, A&A, 509, A50
Chini, R., Hoffmeister, V., Kimeswenger, S., et al. 2004, Nature, 429, 155
Chini, R., Hoffmeister, V. H., Nielbock, M., et al. 2006, ApJ, 645, L61
Commerçon, B., Hennebelle, P., & Henning, T. 2011, ApJ, 742, L9
Davies, B., Lumsden, S. L., Hoare, M. G., Oudmaijer, R. D., & de Wit, W.-J. 2010, MNRAS, 402, 1504
De Pree, C. G., Goss, W. M., Palmer, P., & Rubin, R. H. 1994, ApJ, 428, 670
Federrath, C., Banerjee, R., Clark, P. C., & Klessen, R. S. 2010, ApJ, 713, 269
Fendt, C. 2006, ApJ, 651, 272
Fendt, C., & Čemeljić, M. 2002, A&A, 395, 1045

Fryxell, B., Olson, K., Ricker, P., et al. 2000, ApJS, 131, 273
Furuya, R. S., Cesaroni, R., Codella, C., et al. 2002, A&A, 390, L1
Furuya, R. S., Cesaroni, R., & Shinnaga, H. 2011, A&A, 525, A72
Furuya, R. S., Cesaroni, R., Takahashi, S., et al. 2008, ApJ, 673, 363
Galván-Madrid, R., Keto, E., Zhang, Q., et al. 2009, ApJ, 706, 1036
Galván-Madrid, R., Peters, T., Keto, E. R., et al. 2011, MNRAS, 416, 1033
Garay, G., Rodríguez, L. F., & van Gorkom, J. H. 1986, ApJ, 309, 553
Garmany, C. D., Conti, P. S., & Massey, P. 1980, ApJ, 242, 1063
Girart, J. M., Beltrán, M. T., Zhang, Q., Rao, R., & Estalella, R. 2009, Science, 324, 1408
Girichidis, P., Federrath, C., Banerjee, R., & Klessen, R. S. 2012, MNRAS, 420, 613
Guillet, V., Pineau des Forêts, G., & Jones, A. P. 2011, A&A, 527, A123
Gusdorf, A., Cabrit, S., Flower, D. R., & Pineau Des Forêts, G. 2008, A&A, 482, 809
Guzmán, A. E., Garay, G., Brooks, K. J., Rathborne, J., & Güsten, R. 2011, ApJ, 736, 150
Hennebelle, P., Commerçon, B., Joos, M., et al. 2011, A&A, 528, A72
Ho, P. T. P., & Haschick, A. D. 1981, ApJ, 248, 622
Hollenbach, D. J., Werner, M. W., & Salpeter, E. E. 1971, ApJ, 163, 165
Howard, E. M., Koerner, D. W., & Pipher, J. L. 1997, ApJ, 477, 738
Hunter, T. R., Brogan, C. L., Indebetouw, R., & Cyganowski, C. J. 2008, ApJ, 680, 1271
Jiang, Z., Tamura, M., Hoare, M. G., et al. 2008, ApJ, 673, L175
Johnston, K. G., Shepherd, D. S., Aguirre, J. E., et al. 2009, ApJ, 707, 283
Keto, E., & Klaassen, P. 2008, ApJ, 678, L109
Klaassen, P. D., Wilson, C. D., Keto, E. R., & Zhang, Q. 2009, ApJ, 703, 1308
Klaassen, P. D., Wilson, C. D., Keto, E. R., et al. 2011, A&A, 530, A53
Kobulnicky, H. A., & Fryer, C. L. 2007, ApJ, 670, 747
Königl, A., & Pudritz, R. E. 2000, in Protostars and Planets IV, ed. V. Mannings, A. P. Boss, & S. S. Russell (Tucson: The University of Arizona Press), 759
Krasnopolsky, R., Li, Z.-Y., & Blandford, R. 1999, ApJ, 526, 631
Krumholz, M. R., Klein, R. I., McKee, C. F., Offner, S. S. R., & Cunningham, A. J. 2009, Science, 323, 754
Kuiper, R., Klahr, H., Beuther, H., & Henning, T. 2011, ApJ, 732, 20
—. 2012, A&A, 537, A122
Lii, P., Romanova, M., & Lovelace, R. 2012, MNRAS, 420, 2020
López-Sepulcre, A., Codella, C., Cesaroni, R., Marcelino, N., & Walmsley, C. M. 2009, A&A, 499, 811
Lovelace, R. V. E., Romanova, M. M., & Bisnovatyi-Kogan, G. S. 1999, ApJ, 514, 368
Lynden-Bell, D. 2003, MNRAS, 341, 1360
Machida, M. N., Tomisaka, K., & Matsumoto, T. 2004, MNRAS, 348, L1
Matsumoto, T., & Tomisaka, K. 2004, ApJ, 616, 266
McMullin, J. P., Waters, B., Schiebel, D., Young, W., & Golap, K. 2007, in Astronomical Data Analysis Software and Systems XVI, ed. R. A. Shaw, F. Hill, & D. J. Bell (San Francisco: ASP), 127
Motogi, K., Sorai, K., Habe, A., et al. 2011, PASJ, 63, 31
Najita, J. R., & Shu, F. H. 1994, ApJ, 429, 808
Olmi, L., Cesaroni, R., Neri, R., & Walmsley, C. M. 1996a, A&A, 315, 565
Olmi, L., Cesaroni, R., & Walmsley, C. M. 1996b, A&A, 307, 599
Ouyed, R., & Pudritz, R. E. 1997, ApJ, 482, 712
Owocki, S. 2009, in EAS Publications Series, ed. C. Neiner & J.-P. Zahn, Vol. 39 (EDP Sciences), 223
Peters, T., Banerjee, R., Klessen, R. S., & Mac Low, M.-M. 2011, ApJ, 729, 72
Peters, T., Banerjee, R., Klessen, R. S., et al. 2010a, ApJ, 711, 1017
Peters, T., Klessen, R. S., Mac Low, M.-M., & Banerjee, R. 2010b, ApJ, 725, 134
Peters, T., Mac Low, M.-M., Banerjee, R., Klessen, R. S., & Dullemond, C. P. 2010c, ApJ, 719, 831
Pudritz, R. E., & Norman, C. A. 1983, ApJ, 274, 677
Puga, E., Feldt, M., Alvarez, C., et al. 2006, ApJ, 641, 373
Qin, S.-L., Wang, J.-J., Zhao, G., Miller, M., & Zhao, J.-H. 2008, A&A, 484, 361
Ray, T., Dougados, C., Bacciotti, F., Eislöffel, J., & Chrysostomou, A. 2007, in Protostars and Planets V, ed. B. Reipurth, D. Jewitt, & K. Keil (Tucson: The University of Arizona Press), 231
Reipurth, B., & Bally, J. 2001, ARA&A, 39, 403
Richer, J. S., Shepherd, D. S., Cabrit, S., Bachiller, R., & Churchwell, E. 2000, in Protostars and Planets IV, ed. V. Mannings, A. P. Boss, & S. S. Russell (Tucson: The University of Arizona Press), 867
Riffel, R. A., & Lüdke, E. 2010, MNRAS, 404, 1449
Rijkhorst, E.-J., Plewa, T., Dubey, A., & Mellema, G. 2006, A&A, 452, 907
Romanova, M. M., Ustyugova, G. V., Koldoba, A. V., & Lovelace, R. V. E. 2009, MNRAS, 399, 1802
Schilke, P., Walmsley, C. M., Pineau des Forêts, G., & Flower, D. R. 1997, A&A, 321, 293
Schöier, F. L., van der Tak, F. F. S., van Dishoeck, E. F., & Black, J. H. 2005, A&A, 432, 369
Seifried, D., Banerjee, R., Klessen, R. S., Duffin, D., & Pudritz, R. E. 2011, MNRAS, 417, 1054
Seifried, D., Pudritz, R. E., Banerjee, R., Duffin, D., & Klessen, R. S. 2012, MNRAS, 422, 347
Sewiło, M., Churchwell, E., Kurtz, S., Goss, W. M., & Hofner, P. 2008, ApJ, 681, 350
Shepherd, D. 2005, in Massive star birth: A crossroads of Astrophysics, ed. R. Cesaroni, M. Felli, E. Churchwell, & M. Walmsley (Cambridge University Press), 237
Shepherd, D. S., & Churchwell, E. 1996, ApJ, 472, 225
Shetty, R., Glover, S. C., Dullemond, C. P., & Klessen, R. S. 2011, MNRAS, 412, 1686
Shi, H., Zhao, J.-H., & Han, J. L. 2010, ApJ, 718, L181
Shu, F., Najita, J., Ostriker, E., et al. 1994, ApJ, 429, 781
Shu, F. H., Galli, D., Lizano, S., & Cai, M. J. 2007, in Star-disk interaction in young stars, ed. J. Bouvier & I. Appenzeller (Cambridge University Press), 249
Su, Y.-N., Liu, S.-Y., Chen, H.-R., & Tang, Y.-W. 2012, ApJ, 744, L26
Surcis, G., Vlemmings, W. H. T., Curiel, S., et al. 2011, A&A, 527, A48
Tang, Y.-W., Ho, P. T. P., Girart, J. M., et al. 2009a, ApJ, 695, 1399
Tang, Y.-W., Ho, P. T. P., Koch, P. M., et al. 2009b, ApJ, 700, 251
Tang, Y.-W., Ho, P. T. P., Koch, P. M., & Rao, R. 2010, ApJ, 717, 1262
Tomisaka, K. 1998, ApJ, 502, L163
—. 2002, ApJ, 575, 306
Vaidya, B., Fendt, C., & Beuther, H. 2009, ApJ, 702, 567
Vaidya, B., Fendt, C., Beuther, H., & Porth, O. 2011, ApJ, 742, 56
Vlemmings, W. H. T., Surcis, G., Torstensson, K. J. E., & van Langevelde, H. J. 2010, MNRAS, 404, 134
Watson, C., Churchwell, E., Zweibel, E. G., & Crutcher, R. M. 2007, ApJ, 657, 318
Wilson, T. L., & Rood, R. T. 1994, ARA&A, 32, 191
Wu, Y., Wei, Y., Zhao, M., et al. 2004, A&A, 426, 503
Zapata, L. A., Tang, Y.-W., & Leurini, S. 2010, ApJ, 725, 1091
Zhang, Q., Ho, P. T. P., & Ohashi, N. 1998, ApJ, 494, 636
Zinnecker, H., & Yorke, H. W. 2007, ARA&A, 45, 481